

SceneAdapt: Scene-Based Domain Adaptation for Semantic Segmentation using Adversarial Learning

Daniele Di Mauro^{1,2}, Antonino Furnari¹, Giuseppe Patanè², Sebastiano Battiato¹, and Giovanni Maria Farinella¹

¹Department of Mathematics and Computer Science, University of Catania, Italy

²Park Smart s.r.l., Catania, Italy

Abstract

Semantic segmentation methods have achieved outstanding performance thanks to deep learning. Nevertheless, when such algorithms are deployed to new contexts not seen during training, it is necessary to collect and label scene-specific data in order to adapt them to the new domain using fine-tuning. This process is required whenever an already installed camera is moved or a new camera is introduced in a camera network due to the different scene layouts induced by the different viewpoints. To limit the amount of additional training data to be collected, it would be ideal to train a semantic segmentation method using labeled data already available and only unlabeled data coming from the new camera. We formalize this problem as a domain adaptation task and introduce a novel dataset of urban scenes with the related semantic labels. As a first approach to address this challenging task, we propose SceneAdapt, a method for scene adaptation of semantic segmentation algorithms based on adversarial learning. Experiments and comparisons with state-of-the-art approaches to domain adaptation highlight that promising performance can be achieved using adversarial learning both when the two scenes have different but points of view, and when they comprise images of completely different scenes.

To encourage research on this topic, we made our code available at our web page: [https://iplab.](https://iplab.dmi.unict.it/ParkSmartSceneAdaptation/)

[dmi.unict.it/ParkSmartSceneAdaptation/](https://iplab.dmi.unict.it/ParkSmartSceneAdaptation/).

Keywords: Semantic Segmentation, Domain Adaptation, Scene Adaptation, Adversarial Learning

1 Introduction

Semantic segmentation allows to classify each pixel of an image according to the object it belongs to in the scene. This task is often the first step in scene understanding and is important in many industrial scenarios including video surveillance and traffic analysis (Raymond, 2001; Battiato et al., 2018; Ravi et al., 2016). In recent years, deep learning allowed to push forward the performance of semantic segmentation methods (Badrinarayanan et al., 2017; Long et al., 2015; Zhao et al., 2017b; Chen et al., 2018). However, such approaches generally require to be trained on large quantities of domain-specific labeled data in order to achieve reasonable performance. In practice, deploying a semantic segmentation system often involves collecting domain-specific data and fine-tuning an existing semantic segmentation algorithm pre-trained on large quantities of domain-agnostic data. Moreover, this fine-tuning process (including the collection and labeling of new data) needs to be repeated whenever the target domain changes significantly, e.g., when an existing camera is moved or a new one is introduced in the camera network, due to the different scene layouts induced by the different viewpoints. The significant effort required to collect

and label domain-specific data can slow down the deployment of industrial systems based on semantic segmentation algorithms and prevent them from scaling up.

In this paper, we consider a scene adaptation scenario in which a fixed camera is employed to monitor a urban area. When the system is set up, domain-specific data is collected and labeled. An existing algorithm is hence fine-tuned to perform the semantic segmentation of the scene. In real scenarios, the system is often extended by adding a new camera looking at the same scene from a different point of view or by adding a camera looking at a different scene characterized by the same semantic classes (e.g. a different urban area). After the installation of the new cameras, the existing algorithms need to be adapted to the new views or scenes. The proposed scene adaptation problem is illustrated in Figure 1. The adaptation procedure in such contexts is generally achieved collecting and labeling additional data from the two cameras in order to fine-tune the algorithms in a purely supervised way. However, as observed in previous work (Tzeng et al., 2017; Tsai et al., 2018; Sankaranarayanan et al., 2018), the amount of effort required to collect and label domain-specific data to perform fine-tuning can be reduced using domain adaptation techniques (i.e., trying to bypass the three steps of data collection, labeling and fine-tuning).

We frame the considered scene adaptation task as a Domain Adaptation problem in which labeled images collected using the already installed camera belong to the source domain, whereas unlabeled images collected using the new camera belong to the target domain. We observe that no datasets comprising real images from different cameras looking at the same/similar scenes are available to support our investigation. This is mainly due to the challenges arising when collecting real data in these settings. To overcome these issues and provide a first set of data useful to investigate the proposed problem, we collect and publicly release a novel dataset of urban scenes using the CARLA Urban Driving Simulator (Dosovitskiy et al., 2017). The collected dataset comprises images generated in 3 scene contexts from 6 different



Figure 1: The proposed scene adaptation scenario². A camera S (dark yellow) is installed to monitor a urban space. This initial set up requires the collection and labeling of domain-specific data to optimize an existing semantic segmentation algorithm to the considered task. The system can be extended by adding a camera which observes the same scene from a different point of view S' (blue) or by adding a new camera which observes a different scene S'' (red). In both cases, the existing semantic segmentation algorithms need to be adapted to the new views.

views (2 views per context).

As a first step towards addressing the proposed task, we contribute a method which leverages Adversarial Learning (Goodfellow et al., 2014) to perform scene adaptation. The proposed approach takes advantage only of existing *labeled* data from the source domain and newly collected *unlabeled* images from the target domain. We enforce that the input images can be reconstructed from the produced segmentation maps, while the realness of the reconstructions is imposed through adversarial learning. The reconstructive criterion allows to define a supervised loss for the unlabeled data and acts as a regularizer which encourages the network to learn view invariant representations for small scene elements such as traffic signs and fences. While the proposed approach is conceptually simple, we show that it significantly outperforms a pipeline including the geometric warp of the input images, which suggests that it is appropriate to consider the problem as a domain adaptation

²Underneath photo by Felix Steininger on Unsplash.

task. We hope that the proposed approach may serve as a useful baseline for other works. The method is independent from the specific semantic segmentation network employed and can be regarded to as a general training procedure which allows generalization to unseen views. Experiments show that the proposed approach achieves state of the art performance, surpassing baselines and previous domain adaptation techniques.

The contributions of this work are as follows: 1) we introduce the problem of scene-based domain adaptation for semantic segmentation algorithms; 2) we propose CARLA-SA (Carla-Scene Adaption), a dataset of urban scenes to study the considered domain adaptation problem; 3) we contribute SceneAdapt, a method to perform scene adaptation using adversarial learning, which is shown to outperform baseline and state-of-the-art approaches. This work extends our previous investigation (Di Mauro et al., 2018) introducing a clearer introduction of the proposed method, additional comparisons with state of the art approaches and baselines, as well as an ablation study discussing the impact of each component on the final performance. Moreover, with this paper we publicly release both the collected dataset and the code of the proposed method³.

2 Related Work

Semantic Segmentation Many recent works have proposed semantic segmentation algorithms based on deep learning. Among the most notable recent approaches, Long et al. (2015) proposed fully convolutional networks, which are obtained by adapting existing CNNs for classification to produce dense image segmentation masks. Badrinarayanan et al. (2017) presented SegNet, a semantic segmentation approach based on an encoder-decoder architecture. Chen et al. (2018) combined atrous convolution and atrous spatial pyramid pooling (ASPP) to segment objects at multiple scales, thus capturing both objects and image context. Zhao et al. (2017a) proposed a cascade network to achieve real-time semantic segmentation. Zhao et al. (2017b) introduced PSPNet,

which comprises a novel pyramid pooling module to leverage global contextual information. The scene-adaptation approach presented in this paper can integrate any semantic segmentation method which is trainable end-to-end. In our experiments, we will consider the state-of-the-art PSPNet architecture.

Adversarial learning The proposed approach leverages the paradigm of adversarial learning, originally introduced with Generative Adversarial Networks (GANs) by Goodfellow et al. (2014). In particular, our work is related to the investigations of Isola et al. (2017); Zhu et al. (2017), who addressed the problem of image translation using GANs. The image translation problem assumes the presence of two different domains X and Y . The goal of image translation is to learn a function $F : X \rightarrow Y$ which maps an input $x \in X$ to an output \hat{y} which is indistinguishable from the elements sampled from Y .

Domain Adaptation for Semantic Segmentation The use of domain adaptation techniques for semantic segmentation has also been investigated in past works. Hoffman et al. (2016), proposed a semantic segmentation network to perform global domain alignment with fully convolutional domain adversarial learning. In a subsequent work, Hoffman et al. (2018) proposed to adapt representations at the pixel-level and at the feature-level with cycle-consistency without requiring aligned pairs. This model has been applied to different visual recognition and prediction settings, including the semantic segmentation of road scenes. Sankaranarayanan et al. (2018) designed a domain adaptation method for semantic segmentation composed by an embedding network, a pixel-wise classifier, a generator network and a discriminator network. Tsai et al. (2018) employed a multi-level adversarial network to perform output space domain adaptation at different feature levels. The algorithm consists of two modules: a segmentation network and a discriminator operating at different levels of the network. Some works address the domain gap created by the device used to capture the data Yang et al. (2019) for instance addressed the domain gap between pinhole and omnidirectional perspectives, whereas Xiang et al. (2020) addressed semantic segmentation based on a dual-camera system with different perspectives and overlapped views.

³<http://iplab.dmi.unict.it/SceneAdapt/>.

Romera et al. (2019), focused on the domain gap due to the moment of the day in which a given a scene has been captured.

Our method leverages some of the intuitions presented in these prior works, framing the investigation in the context of the proposed scene-adaptation task.

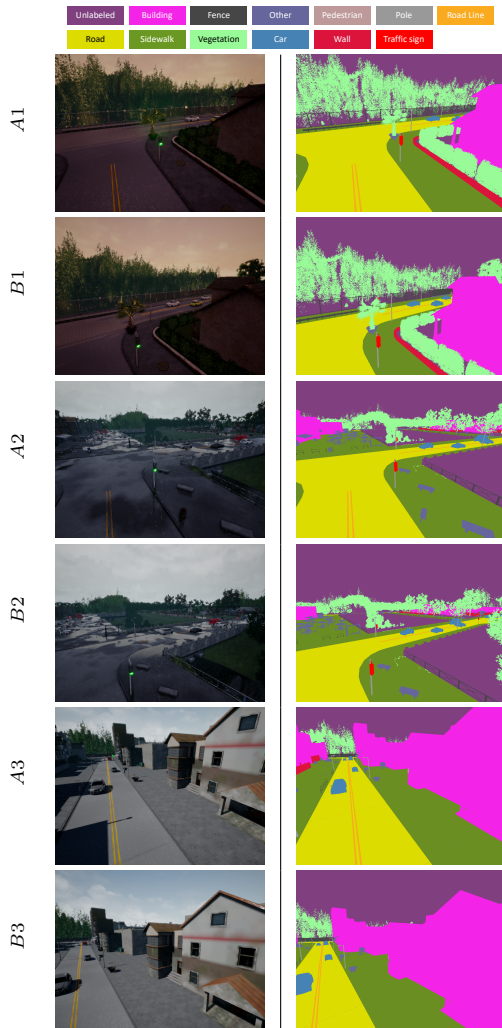


Figure 2: Sample images and ground truth segmentation masks from the 6 data subsets.

3 Dataset

We collected the dataset CARLA-SA using the CARLA Urban Driving Simulator (Dosovitskiy et al., 2017). The simulator has been designed to generate images from the point of view of vehicles for autonomous driving, whereas, to study the scene adaptation problem, we need to collect images of the same scene from different fixed points of view. We achieve this by placing the vehicle which collects the images at predefined locations in the virtual city. To obtain different views of the same scene, for each vehicle we set up multiple cameras at different altitudes, pitch, yaw and roll angles. The vehicle collecting the images does not move during the simulations, while other vehicles and pedestrians are free to move in the scene.

Using this procedure, we collected three episodes in three different scene contexts of the virtual city, which we refer to as “Scene 1”, “Scene 2” and “Scene 3”. Each scene has been captured by two different points of view presenting scene overlap, which we refer to as “View A” and “View B”. The two views differ by an angle of 10° of pitch and by an angle of 10° of yaw. Therefore, the dataset consists of 6 image subsets denoted as “XY”, where X represent the view and Y represents the scene characterizing the subset (e.g., $A1$, $B2$, etc.). Figure 2 reports some examples from the 6 subsets. Each subset is split into a training and a test set. Specifically, for each subset, we randomly pick 60% of the data from training, 20% for validation and 20% for testing.

The dataset contains 5,000 frames acquired at 1 *fps* for each scene-view pair, for a total of 30,000 frames in the whole dataset. Each image has been collected at the resolution of 800×600 pixels. The time of the day and weather has been generated randomly. For each image, the simulator also produces a ground truth semantic segmentation map which associates each pixel of the scene to one of 13 classes: *buildings*, *fences*, *pedestrians*, *poles*, *road-lines*, *roads*, *sidewalks*, *vegetation*, *vehicles*, *walls*, *traffic signs*, *other*, and *unlabeled*.

This dataset allows to consider two types of source-target domain pairs: 1) “point of view adaptation” pairs, composed by two subsets from the same scene context but with different views (e.g., $A1 - B1$, $A2 -$

$B2$, etc. in Figure 2), 2) “scene adaptation” pairs, composed by two subsets belonging to different scene contexts (e.g., $A1 - A2$, $A2 - A3$, etc. in Figure 2).

4 SceneAdapt Method

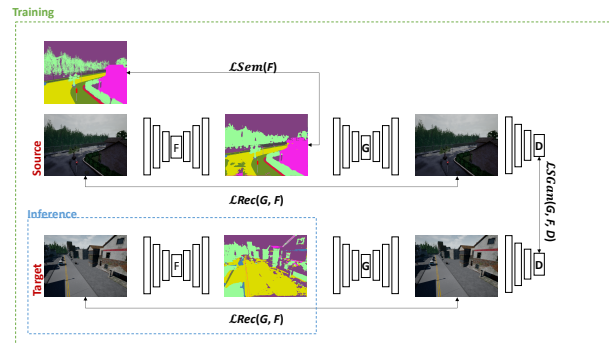


Figure 3: The proposed SceneAdapt architecture to train semantic segmentation networks for scene-based domain adaptation. During the training phase all networks are used employed (green “Training” dashed box), whereas only the part highlighted in blue is used for inference (blue “Inference” dashed box).

We propose SceneAdapt, a method to train a semantic segmentation network using labeled images from the source domain and only unlabeled images from the target domain. Indeed, at test time only the semantic segmentation module is needed to predict segmentation masks from images coming to both domains.

4.1 Proposed Training Architecture

Figure 3 illustrates the proposed training architecture, which consists of a the semantic network to be trained (F), a generative network (G), and a discriminator network (D). The semantic network F predicts semantic segmentation masks for images belonging to both the source and target domains. The ground truth segmentation masks of the source domain can be used to provide direct supervision to F through a semantic segmentation loss. Direct supervision to

F cannot be provided for the target domain, where ground truth segmentation masks are not available. Therefore, we use the generator G to reconstruct the input images from the generated ground segmentation masks and impose that the reconstructed images should be indistinguishable from the original ones. This encourages the semantic segmentation network F to encode details useful for the reconstruction in the produced segmentation masks (e.g., small objects such as traffic lights and cars), which are generally lost in cross-domain testing. The reconstruction requirement is enforced using a reconstruction loss between original and generated images and an adversarial loss which makes use of a discriminator D to improve the performance of the generator G in an adversarial fashion.

Semantic Segmentation Component F is responsible for predicting a segmentation mask for each input image, regardless of the related domain. In our experiments, we implement this module using the PSPNet architecture proposed by Zhao et al. (2017b), which is a state of art model. The network is implemented using a pre-trained ResNet backbone He et al. (2016). We would like to note that, in principle, any semantic segmentation network trainable end-to-end through gradient descent can be used to implement F .

Generator Component G is used to reconstruct the input images from the segmentation masks generated using F . Specifically, the network G takes over the pixel-wise class scores produced by the semantic segmentation network F and generates an RGB image of the same dimensions as the input image. We implement the generator component using the architecture proposed by Johnson et al. (2016), as implemented in Zhu et al. (2017).

Discriminator Component D allows to train the system using adversarial learning. Specifically, the discriminator is trained to distinguish between the input images and the generated ones, whereas the F and G components are jointly trained to “fool” the discriminator, as proposed in Goodfellow et al. (2014). D is implemented considering the PatchGANs architecture used in (Isola et al., 2017; Li and Wand, 2016; Ledig et al., 2016). The network operates on 70×70 overlapping image patches. This

patch-level discriminator architecture has fewer parameters than a full-image discriminator and can be applied to arbitrarily-sized images in a fully convolutional fashion as described in Isola et al. (2017).

4.2 Loss Functions

The overall architecture illustrated in Figure 3 is trained using a composite loss which encourages the network to produce good semantic segmentation masks for both domains. Specifically, the loss combines a semantic segmentation loss, a reconstruction loss and an adversarial loss.

Semantic Segmentation Loss This loss is used to provide direct supervision to F , when it is trained with images from the source domain. The loss is computed as the pixel-wise cross entropy between the inferred probability mask and the ground truth mask. Note that this loss can be applied only to image-label pairs of the source domain, since no ground truth segmentation masks are available for images of the target domain. Specifically, let x be an image from the source domain S , let $F(x)$ be the set of scores produced by the semantic segmentation network, and let $\mathcal{S}(F(x))$ be the softmax of $F(x)$, computed along the class scores independently for each pixel. Let y be the ground truth segmentation mask associated to x , which indicates that a pixel i belongs to class y_i . We define the semantic segmentation loss as follows:

$$\mathcal{L}_{Sem}(F) = \mathbb{E}_{x \sim p_S(x)} \left[- \sum_i \log(\mathcal{S}(F(x))_{i, y_i}) \right], \quad (1)$$

where p_S denotes the distribution of the data of the source domain, i iterates over the pixels of the training image x , \mathcal{S} denotes the softmax function, and $\mathcal{S}(F(x))_{i, y_i}$ denotes the probability predicted for class y_i and pixel i .

Reconstruction Loss As done in Zhu et al. (2017), we use an L_1 loss to enforce the correct reconstruction of the input images starting from the pixel-wise class scores produced by the semantic segmentation network (before Softmax). This loss is calculated for all the input-reconstructed image pairs of both the source and target domains. The reconstruction

loss is defined as follows:

$$\mathcal{L}_{Rec}(G, F) = \mathbb{E}_{x \sim p_{ST}(x)} [\|G(F(x)) - x\|_1], \quad (2)$$

where p_{ST} denotes the distribution of data belonging to both source and target domains, and $\|\cdot\|_1$ denotes the L1 norm. This loss is used to provide indirect supervision to the semantic network F also for the unlabeled images belonging to the target domain, encouraging it to include in the segmentation mask domain-specific details useful for reconstruction.

Adversarial Loss This loss allows to improve the performance of F and G in an adversarial fashion. Specifically, it forces the generator G to produce better reconstructions and overcome the common limitations of regression-based losses for reconstruction purposes (Mathieu et al., 2015). The loss is applied to images generated for both the source and target domain and is defined as follows:

$$\mathcal{L}_{GAN}(G, F, D) = \mathbb{E}_{x \sim p_{ST}(x)} [\log(D(x))] + \quad (3)$$

$$\mathbb{E}_{x \sim p_{ST}(x)} [\log(1 - D(G(F(x))))]. \quad (4)$$

Overall Loss The overall loss used to optimize the whole training architecture is defined as the sum of the three losses discussed in previous sections:

$$\mathcal{L}(G, F, D) = \mathcal{L}_{Sem}(F) + \mathcal{L}_{Rec}(G, F) + \mathcal{L}_{GAN}(G, F, D). \quad (5)$$

5 Experimental Settings and Results

We compare the proposed method with respect to the following baselines and state of the art domain adaptation techniques:

No Adaptation (NA) This baseline is obtained training PSPNet, on the source domain and testing it on the target domain, without adaptation;

Fine Tuning (FT) This is a strong baseline, obtained performing the fine-tuning procedure, i.e., training PSPNet on the target domain using ground truth annotations. It should be noted that, since this strong baseline uses the ground truth annotations, it is reported for reference only.

Geometric Warp (WARP) This baseline tries to model the domain gap through geometrical considerations. In particular, it assumes that an affine transformation \mathcal{H} between the source and target scenes exists and is known. Hence, we test this baseline only in the case of point of view adaptation, where a geometrical correspondence between the scenes can be established. At training time, all images from the source domain are warped using \mathcal{H} in order to match the geometry of the target domain. The same transformation is applied to the ground truth segmentation masks with nearest neighbor interpolation to recover the class of missing points. A PSPNet model is hence trained on the warped images. The network is tested directly on the target domain images, where no warp operation is needed. It should be noted that, as the source images need to be mapped to a higher resolution in order to preserve the scale of the objects appearing in the scene, this baseline is computationally expensive to train.

ASEGNET A domain adaptation approach proposed by Tsai et al. (2018). We use the official implementation provided by the authors for the experiments;

LSD A domain adaptation method proposed by Sankaranarayanan et al. (2018). This method is composed by an encoder with a bottleneck, a decoder, and a semantic decoder. The encoder maps the input image to a spatial embedding space. The first decoder reconstructs the image from the embedded input, whereas the semantic decoder infers the semantic segmentation mask from the embedded input. Note that the main difference between the proposed LSD and the proposed method, is that we do not consider an embedded space. In contrast, we enforce that the produced semantic segmentation masks are sufficient to reconstruct the input. This is equivalent to considering a highly semantic embedding space induced by the softmax predictions. We use the official implementation provided by the authors for the experiments.

We perform two sets of experiments to assess the performance of the proposed method in the contexts of point of view adaptation and general scene adaptation. In the first set of experiments (point of view adaptation), the source and target domains are re-

lated to images acquired in the same scene from different points of view. In the second set of experiments (general scene adaptation), source and target domains are related to images acquired in different, non-overlapping scenes.

All algorithms have been trained till convergence. The weights of the best epoch (according to the validation set) are selected for the evaluation. For the baselines (i.e. NA and FT) and our method, we use PSPNet with Resnet-101 as backbone and we optimize using Stochastic Gradient Descent (SGD) with momentum equal to 0.9, initial learning rate equal to 0.007, weight decay equal to $(1 - i/3750)^{0.9}$ (where i is the current iteration, and 3750 is the total number of iterations) and batch size equal to 8. The proposed method is optimized using the Adam optimizer, with initial learning rate equal to 0.0002 and batch size equal to 1. LSD (Sankaranarayanan et al., 2018) is trained using SGD with momentum equal to 0.9, initial learning equal to $1.0 \cdot 10^{-5}$ and weight decay coefficient equal to 0.0005. ASENET (Tsai et al., 2018) is trained using SGD with momentum 0.9, initial learning equal to $2.5 \cdot 10^{-4}$ and weight decay coefficient equal to 0.0005. All the results have been evaluated using per-class accuracy (c_{acc}) and mean intersection over union (m_{iou}) as defined in Long et al. (2015).

5.1 Comparison with the state of the art

Table 1 reports the point of view adaptation results⁴. Best per-row results are highlighted in bold numbers in the table. The cases in which the best method outperforms the *FT* strong baseline are underlined. The table reports the average results, as well as the breakdown according to the different classes. The proposed method outperforms with a good margin all competitors (in average) considering both per-class accuracy and mean intersection over union. Interestingly, while the strong baseline *FT* reports in general the best results, the proposed method outperforms *FT* for some classes such as “Fences”, “Pedes-

⁴The results are averaged over the following source-target image pairs: $A1 - B1$, $A2 - B2$, $A3 - B3$, $B1 - A1$, $B2 - A2$, $B3 - A3$.

Table 1: Point of view adaptation results.

PER-CLASS ACCURACY					
	NA	ASEGNET	LSD	SceneAdapt	FT
Average	0.53	0.52	0.59	0.72	0.69
Unlabeled	0.27	0.80	0.74	0.90	0.96
Buildings	0.96	0.93	0.53	0.95	0.98
Fences	0.28	0.36	0.58	0.55	0.50
Other	0.29	0.32	0.56	0.60	0.46
Pedestrians	0.21	0.04	0.11	0.53	0.21
Poles	0.05	0.08	0.44	0.25	0.22
Road-lines	0.36	0.38	0.55	0.48	0.44
Roads	0.96	0.88	0.59	0.93	0.98
Sidewalks	0.97	0.88	0.73	0.93	0.98
Vegetation	0.89	0.72	0.77	0.82	0.85
Vehicles	0.66	0.48	0.45	0.94	0.84
Walls	0.75	0.83	0.88	0.82	0.88
T. Signs	0.20	0.13	0.78	0.68	0.73
MEAN INTERSECTION OVER UNION					
Average	0.32	0.37	0.34	0.57	0.64
Unlabeled	0.26	0.75	0.48	0.85	0.91
Buildings	0.74	0.87	0.49	0.93	0.98
Fences	0.13	0.15	0.33	0.42	0.42
Other	0.22	0.10	0.25	0.50	0.42
Pedestrians	0.09	0.03	0.09	0.13	0.19
Poles	0.04	0.02	0.17	0.20	0.17
Road-lines	0.20	0.03	0.10	0.36	0.34
Roads	0.55	0.82	0.41	0.86	0.95
Sidewalks	0.76	0.66	0.48	0.88	0.92
Vegetation	0.52	0.49	0.64	0.71	0.74
Vehicles	0.23	0.37	0.33	0.26	0.78
Walls	0.28	0.52	0.31	0.71	0.83
T. Signs	0.16	0.03	0.39	0.63	0.70

Table 2: Results of the WARP baseline for the A1-B1 pair.

	Per Class Accuracy	MIoU
NA	0.47	0.43
WARP	0.58	0.46
SceneAdapt	0.75	0.62
FT	0.72	0.66

trians”, “Vehicles” and “T. Signs”. This suggests that a) the proposed training architecture benefits from joint domain training, as compared to training only with data coming from one domain (as in FT) and b) the proposed method can effectively prevent over-fitting improving the segmentation of small objects. Similar gains can be observed for the mean intersection over union measure. Table 2 compares the performance of the WARP baseline with respect to NA, FT and the proposed method. Please note that, since the WARP baseline is very computationally expensive, we perform these experiments only on the A1-B1 pair. It is worth noting that beside being very computationally expensive to train, the WARP baseline only allows to obtain minor improvements NA, reaching sub-optimal performance with respect to the proposed approach. This suggests that, while a geometric prior can be helpful, the proposed framework implicitly allows to learn some of the differences in the scene layouts arising from different points of view.

Table 3: Scene adaptation results.

PER-CLASS ACCURACY					
	NA	ASEGNET	LSD	SceneAdapt	FT
Average	0.27	0.37	0.32	0.34	0.68
Unlabeled	0.53	0.54	0.39	0.69	0.23
Buildings	0.09	0.18	0.17	0.25	0.99
Fences	0.07	0.03	0.25	0.01	0.52
Other	0.02	0.07	0.02	0.00	0.70
Pedestrians	0.05	0.01	0.03	0.13	0.38
Poles	0.03	0.11	0.25	0.03	0.25
Road-lines	0.13	0.66	0.49	0.52	0.43
Roads	0.84	0.78	0.75	0.77	0.99
Sidewalks	0.67	0.69	0.67	0.50	0.98
Vegetation	0.41	0.22	0.39	0.49	0.94
Vehicles	0.61	0.57	0.35	0.81	0.89
Walls	0.00	0.00	0.00	0.00	0.94
T. Signs	0.04	0.99	0.73	0.18	0.65
MEAN INTERSECTION OVER UNION					
Average	0.19	0.18	0.20	0.22	0.47
Unlabeled	0.30	0.46	0.17	0.50	0.22
Buildings	0.07	0.09	0.25	0.25	0.90
Fences	0.06	0.01	0.02	0.01	0.21
Other	0.02	0.01	0.01	0.00	0.40
Pedestrians	0.03	0.01	0.03	0.02	0.15
Poles	0.01	0.01	0.08	0.02	0.25
Road-lines	0.13	0.07	0.27	0.40	0.33
Roads	0.62	0.71	0.65	0.59	0.88
Sidewalks	0.45	0.44	0.40	0.43	0.88
Vegetation	0.28	0.10	0.23	0.33	0.54
Vehicles	0.40	0.48	0.25	0.21	0.71
Walls	0.00	0.00	0.00	0.00	0.71
T. Signs	0.04	0.00	0.31	0.16	0.07

Table 3 reports the scene adaptation results⁵. The proposed method outperforms all competitors in the case of mean intersection over union and achieves state-of-the-art results in the case of per-class accuracy. The results highlight that general scene adaptation is much more difficult than point of view adaptation. Specifically, the proposed method tends to achieve sub-optimal results as compared to the FT strong baseline. This suggests that, due to the radical change of the image layout due to the very different scenes, the proposed method is not always able to accurately segment small objects such as “pedestrians” and “traffic lines”, albeit it generally improves over the NA baseline. A closer comparison between the LSD method and the proposed approach suggests that using the embedding space induced by the softmax predictions as done by our method is beneficial in the view adaptation scenario for almost all classes with respect to the mean intersection over union measure. In the scene adaptation scenario, our embedding works better with larger classes such as “vegetation”.

Figure 4 reports some qualitative examples of the compared methods on the tasks of view and scene

⁵These results are averaged over the following source-target image pairs: A1 – A2, A1 – A3, A2 – A1, A2 – A3, A3 – A1, A3 – A2.

adaptation.

5.2 Ablation study

To assess the contribution of the reconstruction and adversarial losses described in Section 4.2, we tested three versions of the proposed method on the $A1-B1$ pair for view adaptation and on the $A1-A2$ pair for scene adaptation. Each considered version of the proposed method is trained using different combinations of loss functions as it is shown in Table 4. From the results, it can be observed that dropping the adversarial term in the loss function allows to obtain a boost of +2% in per-class accuracy and +5% in mean intersection over union, whereas dropping the reconstruction term yields worse results. Conversely, for general scene adaptation, the L1 reconstruction term has marginal importance, while combining both reconstruction and adversarial losses leads to the best results. These observations suggest that the L1 term can impose a strong geometric prior, which is useful in the case of point of view adaptation, where the scenes present similar, yet distinct, layouts. When geometric layouts are more diverse, as in the case of scene adaptation, the adversarial term is more beneficial and can overcome the “regression-to-the-mean” effect which could be induced by the L1 loss.

We also assessed if the proposed method allows to improve segmentation results on the source domain thanks to the additional unlabeled images coming from the target domain seen during the training phase. To assess generalization in the case of point of view adaptation, we trained the proposed method on the training sets of the source-target pair $A1-B1$ and tested it on the test set of $A1$ (the source domain). Table 5 compares the results with respect to the NA baseline. As can be noted, the proposed method allows to improve performance on the source domain in all cases. This suggests a regularizing effect induced by the use of unlabeled images from the target domain. Table 6 further compares the proposed SceneAdapt method with respect to the NA baseline reporting per-class measures. Interestingly, most of the improvement is obtained with respect to classes denoting small scene elements, such as “fences” (from 0.4/0.31 to 0.63/0.44 - Per-class Acc./Mean IoU) and

“pedestrians” (from 0.16/0.15 to 0.41/0.27), which are the most sensitive to the changes of points of view. This suggests that the proposed approach successfully encourages the semantic segmentation network to focus on task-relevant details.

6 Conclusion

We have investigated the problem of scene-based domain adaptation for semantic segmentation by defining two adaptation scenarios: point of view adaptation and scene adaptation. To this aim, we collected a dataset of urban scenes and proposed a novel architecture to perform scene and point of view semantic segmentation adaptation using adversarial learning. Experiments show that the proposed method greatly reduces over-fitting in both point of view and scene adaptation and outperforms baselines and other state-of-the-art methods. Future work can be devoted to combining explicit geometric priors (as in the case of the WARP baseline), with the adversarial framework adopted by the proposed method. in the case of point of view adaptation.

References

- Badrinarayanan, V., Kendall, A., and Cipolla, R. (2017). Segnet: A deep convolutional encoder-decoder architecture for image segmentation. *IEEE Transactions on Pattern Analysis and Machine Intelligence*.
- Battiatto, S., Farinella, G. M., Gallo, G., and Giudice, O. (2018). On-board monitoring system for road traffic safety analysis. *Computers in Industry*, 98:208 – 217.
- Chen, L. C., Papandreou, G., Kokkinos, I., Murphy, K., and Yuille, A. L. (2018). Deeplab: Semantic image segmentation with deep convolutional nets, atrous convolution, and fully connected crfs. *IEEE Transactions on Pattern Analysis and Machine Intelligence*, 40(4):834–848.
- Di Mauro, D., Furnari, A., Patanè, G., Battiatto, S., and Farinella, G. M. (2018). Scene adapta-

Table 4: Results of the ablation study.

Loss	Adaptation	C _{acc}	m _{iou}
$\mathcal{L}_{SemS}(F) + \mathcal{L}_{Rec}(G, F)$	point of view	0.77	0.67
$\mathcal{L}_{SemS}(F) + \mathcal{L}_{GAN}(G, F, D)$	point of view	0.71	0.55
$\mathcal{L}_{SemS}(F) + \mathcal{L}_{Rec}(G, F) + \mathcal{L}_{GAN}(G, F, D)$	point of view	0.75	0.62
$\mathcal{L}_{SemS}(F) + \mathcal{L}_{Rec}(G, F)$	scene	0.33	0.20
$\mathcal{L}_{SemS}(F) + \mathcal{L}_{GAN}(G, F, D)$	scene	0.38	0.24
$\mathcal{L}_{SemS}(F) + \mathcal{L}_{Rec}(G, F) + \mathcal{L}_{GAN}(G, F, D)$	scene	0.39	0.24

Table 5: Improvement on the source domain.

Source	Target	Adaptation	Method	Measure	Test Results
A1	-	-	No Adaptation	Per Class Accuracy	0.70
A1	-	-	No Adaptation	Mean IoU	0.64
A1	B1	point of view	SceneAdapt	Per Class Accuracy	0.74
A1	B1	point of view	SceneAdapt	Mean IoU	0.65
A1	A2	scene	SceneAdapt	Per Class Accuracy	0.75
A1	A2	scene	SceneAdapt	Mean IoU	0.66

Table 6: Results on the source domain for point of view adaptation.

	PER-CLASS ACC.		MEAN IoU	
	NA	SceneAdapt	NA	SceneAdapt
Average	0.69	0.76	0.64	0.64
Unlabeled	0.77	0.79	0.70	0.70
Buildings	0.98	0.97	0.97	0.84
Fences	0.40	0.63	0.31	0.44
Other	0.65	0.83	0.50	0.68
Pedestrians	0.16	0.41	0.15	0.27
Poles	0.15	0.45	0.14	0.32
Road-lines	0.43	0.67	0.39	0.52
Roads	0.99	0.92	0.97	0.88
Sidewalks	0.97	0.85	0.93	0.73
Vegetation	0.94	0.90	0.78	0.77
Vehicles	0.88	0.83	0.84	0.73
Walls	0.96	0.73	0.90	0.69
T. Signs	0.76	0.93	0.74	0.76

tion for semantic segmentation using adversarial learning. In *15th IEEE International Conference on Advanced Video and Signal Based Surveillance, AVSS 2018, Auckland, New Zealand, November 29 - November 30, 2018*. IEEE.

Dosovitskiy, A., Ros, G., Codevilla, F., Lopez, A., and Koltun, V. (2017). CARLA: An open urban driving simulator. In *Proceedings of the 1st Annual Conference on Robot Learning*, pages 1–16.

Goodfellow, I., Pouget-Abadie, J., Mirza, M., Xu, B., Warde-Farley, D., Ozair, S., Courville, A., and Bengio, Y. (2014). Generative adversarial nets. In *Advances in neural information processing systems*, pages 2672–2680.

He, K., Zhang, X., Ren, S., and Sun, J. (2016). Deep residual learning for image recognition. In *Proceedings of the IEEE conference on computer vision and pattern recognition*, pages 770–778.

Hoffman, J., Tzeng, E., Park, T., Zhu, J.-Y., Isola, P., Saenko, K., Efros, A., and Darrell, T. (2018). CyCADA: Cycle-consistent adversarial domain adaptation. In Dy, J. and Krause, A., editors, *Proceedings of the 35th International Conference on Machine Learning*, volume 80 of *Proceedings of Machine Learning Research*, pages 1994–2003, Stockholmssan, Stockholm Sweden. PMLR.

Hoffman, J., Wang, D., Yu, F., and Darrell, T. (2016). Fcns in the wild: Pixel-level adversarial and constraint-based adaptation. *arXiv preprint arXiv:1612.02649*.

Isola, P., Zhu, J.-Y., Zhou, T., and Efros, A. A. (2017). Image-to-image translation with conditional adversarial networks. In *Proceedings of the IEEE Conference on Computer Vision and Pattern Recognition*, pages 1125–1134.

Johnson, J., Alahi, A., and Fei-Fei, L. (2016). Perceptual losses for real-time style transfer and super-resolution. In *European Conference on Computer Vision*, pages 694–711. Springer.

Ledig, C., Theis, L., Huszár, F., Caballero, J., Cunningham, A., Acosta, A., Aitken, A., Tejani, A., Totz, J., Wang, Z., et al. (2016). Photo-realistic single image super-resolution using a generative adversarial network. *arXiv preprint*.

Li, C. and Wand, M. (2016). Precomputed real-time texture synthesis with markovian generative adver-

- sarial networks. In *European Conference on Computer Vision*, pages 702–716. Springer.
- Long, J., Shelhamer, E., and Darrell, T. (2015). Fully convolutional networks for semantic segmentation. In *Proceedings of the IEEE conference on computer vision and pattern recognition*, pages 3431–3440.
- Mathieu, M., Couprie, C., and LeCun, Y. (2015). Deep multi-scale video prediction beyond mean square error. *arXiv preprint arXiv:1511.05440*.
- Ravì, D., Bober, M., Farinella, G. M., Guarnera, M., and Battiato, S. (2016). Semantic segmentation of images exploiting dct based features and random forest. *Pattern Recognition*, 52:260–273.
- Raymond, J.-F. (2001). Traffic analysis: Protocols, attacks, design issues, and open problems. In *Designing Privacy Enhancing Technologies*, pages 10–29.
- Romera, E., Bergasa, L. M., Yang, K., Alvarez, J. M., and Barea, R. (2019). Bridging the day and night domain gap for semantic segmentation. In *2019 IEEE Intelligent Vehicles Symposium (IV)*, pages 1312–1318. IEEE.
- Sankaranarayanan, S., Balaji, Y., Jain, A., Nam Lim, S., and Chellappa, R. (2018). Learning from synthetic data: Addressing domain shift for semantic segmentation. In *The IEEE Conference on Computer Vision and Pattern Recognition (CVPR)*.
- Tsai, Y.-H., Hung, W.-C., Schuler, S., Sohn, K., Yang, M.-H., and Chandraker, M. (2018). Learning to adapt structured output space for semantic segmentation. In *The IEEE Conference on Computer Vision and Pattern Recognition (CVPR)*.
- Tzeng, E., Hoffman, J., Saenko, K., and Darrell, T. (2017). Adversarial discriminative domain adaptation. In *2017 IEEE Conference on Computer Vision and Pattern Recognition (CVPR)*, pages 2962–2971.
- Xiang, Z., Bao, A., Li, J., and Su, J. (2020). Boosting real-time driving scene parsing with shared semantics. *IEEE Robotics and Automation Letters*, 5(2):596–603.
- Yang, K., Hu, X., Bergasa, L. M., Romera, E., and Wang, K. (2019). Pass: Panoramic annular semantic segmentation. *IEEE Transactions on Intelligent Transportation Systems*.
- Zhao, H., Qi, X., Shen, X., Shi, J., and Jia, J. (2017a). Icnnet for real-time semantic segmentation on high-resolution images. *CoRR*, abs/1704.08545.
- Zhao, H., Shi, J., Qi, X., Wang, X., and Jia, J. (2017b). Pyramid scene parsing network. In *IEEE Conf. on Computer Vision and Pattern Recognition (CVPR)*, pages 2881–2890.
- Zhu, J.-Y., Park, T., Isola, P., and Efros, A. A. (2017). Unpaired image-to-image translation using cycle-consistent adversarial networks. In *Computer Vision (ICCV), 2017 IEEE International Conference on*.

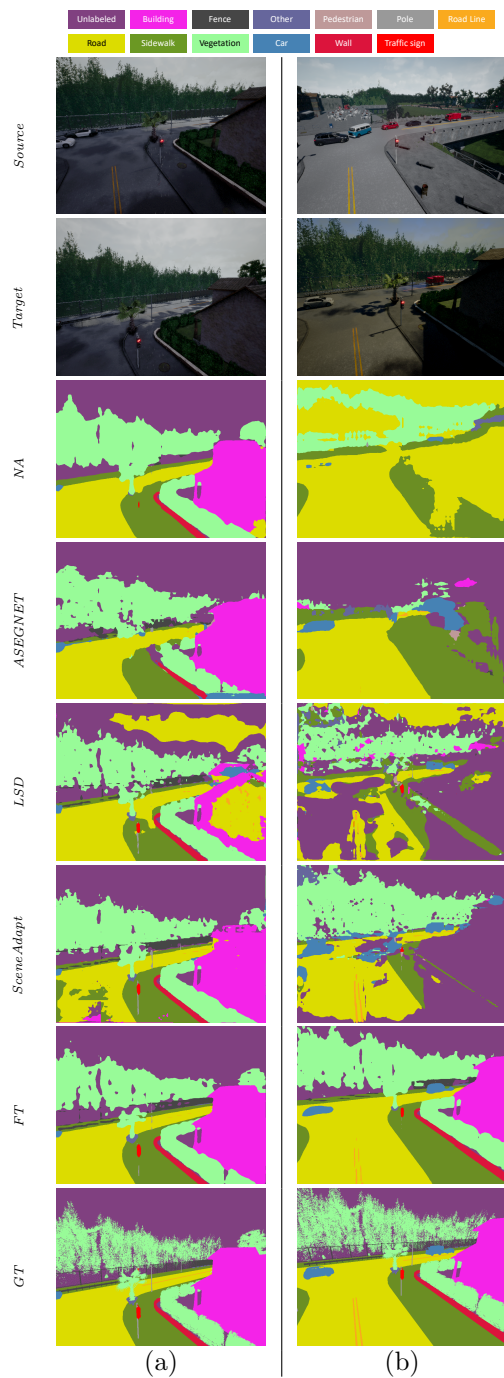


Figure 4: Qualitative comparisons of the considered method on the view adaptation (a) and scene adaptation (b) tasks.